A SURVEY OF NEARBY MAIN-SEQUENCE STARS FOR SUBMILLIMETER EMISSION

E. K. Holmes[1]

Jet Propulsion Laboratory, MS 169-506, California Institute of Technology, 4800 Oak Grove Drive, Pasadena, CA 91109;
holmes@jpl.nasa.gov

H. M. Butner

Submillimeter Telescope Observatory, Steward Observatory, University of Arizona, Tucson, AZ 85721;
hbutner@as.arizona.edu

AND

S. B. Fajardo-Acosta and L. M. Rebull

SITF Science Center, MS 220-6, California Institute of Technology, 1200 East California Boulevard,
Pasadena, CA 91125; fajardo@ipac.caltech.edu, rebull@ipac.caltech.edu

ABSTRACT

We searched for submillimeter emission around 10 Vega-type stars and one Herbig Ae star with the four-color bolometer at 1300 μm and the 19 channel bolometer array at 870 μm using the Heinrich Hertz Telescope at the Submillimeter Telescope Observatory. All of our sources were undetected at 870 μm. In the case of HD 131156, we have a 3 σ detection at 1300 μm. We report a flux of 6.25 ± 1.88 mJy for the HD 131156 disk and a corresponding dust mass of 2.4 ± 0.7 lunar masses. However, we did not detect HD 131156 at 870 μm, so we are cautious about the 1300 μm detection. We performed follow-up infrared observations of HD 131156 using MIRLIN at the Palomar 200 inch telescope, which resolved both components of the binary. The data are photospheric, implying that the system does not have a hot, inner dust component. We report submillimeter upper limits on fluxes for the remaining systems.

Key words: circumstellar matter — submillimeter radiation — surveys

1. INTRODUCTION

The *Infrared Astronomical Satellite* (*IRAS*) detected excess far-infrared emission, at wavelengths of 60 and 100 μm, from more than 15% of all nearby main-sequence A–K stars, indicating the presence of circumstellar material (Backman & Paresce 1993; Elachi et al. 1996). Recent advances in instrumentation have allowed detailed observational maps to be made of a small fraction of these infrared-excess stars revealing disks of circumstellar material, termed planetary debris disks, at both infrared (Koerner et al. 1998; Telesco et al. 2000) and submillimeter (Holland et al. 1998; Greaves et al. 1998) wavelengths. Some of these debris disks show ringlike structures (ϵ Eri) or other asymmetries (β Pic, Fomalhaut, Vega, and HR 4796).

There is a possible connection between the structure in evolved circumstellar disks and the presence of planets (Backman & Paresce 1993; Dermott et al. 1999b), with our own inner planetary debris disk, the zodiacal cloud, being a proven example. Asymmetries in such a disk could be diagnostic of planets that would otherwise be undetectable. Dynamical models of circumstellar disks have been made for the purpose of linking asymmetric structures that arise in planetary debris disks to the presence of planets in the systems (Liou & Zook 1999; Holmes et al. 1999; Dermott et al. 1999b). The models are based on the numerical integration of asteroidal particles. The dynamical evolution of these particles is followed from source to sink with Poynting-Robertson light drag, solar wind drag, radiation pressure, and the effects of planetary gravitational perturbations included. These unique modeling techniques, originally developed to study the influence of the planets and the

Hirayama asteroid families (Dermott et al. 1999a) on the zodiacal cloud, have been extended to produce theoretical exosolar system dust clouds from varying input parameters.

It is our ultimate goal to extend these infrared models into the submillimeter regime (300 μm $\lesssim \lambda \lesssim$ 1000 μm). The cool dust ($T \sim 50$ K) detected in the submillimeter regime lies far (30 AU to hundreds of AU) from the central star. This location is most analogous to the Kuiper belt in our solar system (Backman & Paresce 1993), which is home to an estimated $\sim 10^5$ Kuiper belt objects (KBOs) with a diameter ≥ 100 km located within 30–50 AU (Jewitt, Luu, & Trujillo 1998). In the asteroid belt, collisions between asteroids supply dust particles to the zodiacal cloud, the Sun's inner dust disk, which is visible at optical and infrared wavelengths. By comparison, it has been postulated that collisions between KBOs could initiate a collisional cascade producing a Kuiper dust disk, which would be the second brightest feature of the solar system from an exosolar perspective (Landgraf et al. 2002). From a modeling perspective, far-infrared and submillimeter observations are very interesting because they can be compared with the Kuiper disk.

Submillimeter observational maps of planetary debris disks have been limited to a small number of systems: β Pic, Vega, Fomalhaut (Holland et al. 1998), and ϵ Eri (Greaves et al. 1998). *IRAS* detected very strong far-infrared excesses from all of these nearby main-sequence stars (Gillett 1986; Backman & Paresce 1993) and also resolved them spatially (Backman & Paresce 1993; Aumann & Good 1990). As a result, these four stars have been studied extensively at a number of different wavelengths. However, from a statistical standpoint, we need more detections—and ultimately maps—to claim a broad knowledge of debris disks as a whole, especially considering that upward of 15% of all main-sequence A–K stars have detectable infrared excesses.

---

[1] National Research Council Resident Research Associate.

TABLE 1
SOURCES OBSERVED AT THE SUBMILLIMETER TELESCOPE OBSERVATORY

Star	Name	R.A. (J2000.0)	Decl. (J2000.0)	Distance (pc)	Spectral Type	m_V
HD 10700	τ Cet	01 44 09.99	−15 56 57.9	3.65	G8 V	3.50
HD 165341................		18 05 26.36	+02 30 52.9	5.09	K0 V	4.03
HD 185144................	σ Dra	19 32 15.59	+69 41 09.6	5.77	K0 V	4.67
HD 4614[a]	η Cas A	00 48 59.07	+57 49 23.7	5.95	G3 V (K7 V)	3.46 (7.51)
HD 131156[a]	ξ Boo A	14 51 22.73	+19 06 08.9	6.70	G8 V (K4 V)	4.53 (6.82)
HD 32923		05 07 25.07	+18 38 41.1	15.9	G4 V	4.92
HD 192425................	ρ Aql	20 14 16.34	+15 11 48.2	47.1	A2 V	4.95
HD 82189	22 UMa	09 34 52.70	+72 12 23.9	49.9	F7 V	5.77
HD 37357[a]		05 37 46.96	−06 42 30.2	∼480	A0 Ve	6.05[b]
HD 39415		05 54 41.54	+44 30 08.0		F5 V	8.41
HD 102647................	β Leo	11 49 05.26	14 34 25.16	11.1	A3 V	2.13

NOTE.—Units of right ascension are hours, minutes, and seconds, and units of declination are degrees, arcminutes, and arcseconds. The sources were selected from the *SIRTF* Science Requirements Document in Simmons & Werner 1997 and from Oudmaijer et al. 1992. The distances in the table were derived from the *Hipparcos* Catalog of ESA 1997 for all sources except for HD 37357. *Hipparcos* parallaxes have an error of about 0.8 mas for a typical star at 20 pc. HD 37357 is a Herbig Ae star in a double or multiple system located in Lynds 1641, the nearest giant molecular cloud at a distance of 480 pc, as in Strom et al. 1989. Spectral types were obtained from SIMBAD except for HD 4614 and HD 131156, where they were obtained from Fernandes et al. 1998. The spectral types in parentheses are those of the companion stars. Visual magnitudes were obtained from *Hipparcos* for all of the sources for which data were available. For the five stars (HD 10700, HD 165341, HD 4614 B, HD 37357, and HD 39415) with no *Hipparcos* visual magnitude, m_V was obtained from SIMBAD.

[a] Binary or multiple.
[b] Corrected for extinction with $A_V = 2.8$; see Strom et al. 1989.

We embarked on a submillimeter survey of debris disk candidates—a small selection of nearby (≤ 50 pc) main-sequence stars, which are shown in Table 1. From our survey, we obtain upper limits on the fluxes and limits on the dust masses for our candidate stars. These limits allow us to constrain the spectral energy distributions (SEDs) of the stars at 870 and 1300 μm, which will prove useful to upcoming missions such as the *Space Infrared Telescope Facility* (*SIRTF*). *SIRTF* will observe in the infrared with unprecedented sensitivity, but the longest wavelength at which it will observe is 160 μm. It is therefore important to supplement *SIRTF* observations with ground-based observations of the same set of candidate stars at wavelengths longer than 160 μm.

All of our sources were undetected at 870 μm, and all but one were undetected at 1300 μm. In the case of our one 1300 μm detection, HD 131156 (ξ Boo A or HR 5544), we have a 3 σ detection and we report a flux of 6.25 ± 1.88 mJy. From this flux, we derive a dust mass of 2.4 ± 0.7 lunar masses for the system. However, since we did not have a corresponding detection at 870 μm using the 19 channel bolometer, which is more sensitive than the four-color bolometer with which the 1300 μm observations were taken, we are cautious about the 1300 μm detection.

2. SUBMILLIMETER OBSERVATIONS

We observed a total of 11 stars at the 10 m Heinrich Hertz Telescope of the Submillimeter Telescope Observatory (SMTO) located on Mount Graham in Arizona. We searched for submillimeter flux around our candidate stars with the four-color bolometer on 1999 March 19–24 and 1999 December 9–13 at 1300 μm. We completed our survey on 2000 December 14–16 using the 19 channel bolometer array at 870 μm.

In 1999 March 19–24 and December 9–13, we used the four-color bolometer facility instrument, with central wavelengths at 1300, 870, 450, and 350 μm and a bandwidth of approximately 50 GHz. The half-power beam width at 1300 μm is approximately 35″, which is slightly larger than the diffraction limit of 33″. We made approximately 10 pointing observations per night, to achieve an absolute pointing accuracy of 2″–3″. Continuum on/off measurements of each source were made with a beam throw of ± 100″ in azimuth during the March observing run and a beam throw of ± 60″ in 1999 December. Each continuum scan was composed of 10 subscans, having on- and off-source scans of 30 s each. Total on-source integration times are listed in Table 2. The scans were calibrated using continuum on/off measurements on Venus, Mars, Saturn, and Uranus as well as known secondary submillimeter calibrators: K3-50, W3(OH), NGC 7538 IRS 1, G45.1, and CRL 618 (Sandell 1994). Observations of standards during the spring of 1997 found the 1300 μm noise-equivalent flux density (NEFD) equal to 0.6–0.8 Jy s$^{-1/2}$. We observed 10 Vega-type stars and one Herbig Ae star, HD 37357 (see Table 2).

On 2000 December 14–16, we used the newly installed 19 channel bolometer array, developed at the Max-Planck-Institut für Radioastronomie, Bonn, to observe eight Vega-type stars and one Herbig Ae star (see Table 2). The array consists of 19 individual broadband continuum receivers, each with a central wavelength of 0.87 mm (345 GHz). Eighteen of the channels form two concentric hexagons around the central channel. The NEFD level for the array is approximately 0.6 Jy s$^{-1/2}$. Continuum on/off measurements of each source were made with a beam throw of ± 50″ in azimuth. Each continuum scan was composed of 20 subscans, having on- and off-source scans of 10 s each. Total on-source integration times are listed in Table 2. The scans were calibrated using continuum on/off measurements of Venus, Mars, and Saturn as well as known secondary submillimeter

TABLE 2
Flux or 3 σ Upper Limits for the Flux

	870 μm (19 Channel Bolometer)			1300 μm (Four-Color Bolometer)		
Star	On-Source Integration Time	S/N	3 σ Limit or Flux (mJy)	On-Source Integration Time	S/N	3 σ Limit or Flux (mJy)
HD 10700	47 minutes	+1.94	<19.8			
HD 165341...............				1 hr 30 minutes	+0.94	<8.85
HD 185144...............	47 minutes	+0.043	<37.53	2 hr 35 minutes	−1.11	<3.81
HD 4614	50 minutes	−0.0085	<26.04	40 minutes	−2.10	<23.52
HD 131156...............	1 hr 27 minutes	+0.35	<17.28	3 hr	+3.33	6.25 ± 1.88
HD 32923	30 minutes	+1.53	<38.52	30 minutes	−1.34	<12.60
HD 192425...............	17 minutes	+1.39	<33.30	1 hr 25 minutes	−1.38	<7.95
HD 82189				1 hr 55 minutes	−0.72	<8.91
HD 37357	30 minutes	−1.23	<38.70	20 minutes	+0.29	<26.64
HD 39415	1 hr 10 minutes	+0.92	<18.75	55 minutes	+1.53	<10.68
HD 102647...............	1 hr	+0.17	<20.91	1 hr 20 minutes	+0.30	<8.85

calibrators: K3-50, W3(OH), W75N, and G45.1 (Sandell 1994). Additional observations of HD 131156 taken at Palomar in the mid-infrared are discussed in § 5.

2.1. *Selection Criteria*

We selected our stars from two sources: the *SIRTF* Science Requirements Document (SRD) (Simmons & Werner 1997) and a list of Smithsonian Astrophysical Observatory (SAO) stars having infrared excesses in the *IRAS* Point Source Catalog compiled by Oudmaijer et al. (1992). Five of our candidate stars are listed in the *SIRTF* SRD as candidate stars for possessing planetary debris disks: HD 10700 (τ Cet), HD 165341, HD 185144 (σ Dra), HD 4614 (η Cas A), and HD 131156 (ξ Boo A) (Simmons & Werner 1997). These are five of the closest stars (located within 6.8 pc) with spectral types between G0 V and K0 V and luminosities similar to solar ($0.37\ L_\odot < L < 1.24\ L_\odot$). Aumann & Good (1990) found statistical evidence that the typical G dwarf in the solar neighborhood has a weak 100 μm excess, perhaps from cold circumstellar dust. Studying nearby stars ($d \leq 10$ pc) is advantageous since it increases the probability of a submillimeter detection for systems possessing a small amount of dust. It allows tight limits on dust mass to be placed on any nondetections since the dust mass is proportional to the square of the frequently uncertain distance.

The remaining candidate stars, HD 102647 (β Leo), HD 192425 (ρ Aql), HD 82189 (22 UMa), HD 32932, HD 37357, and HD 39415, were acquired from a list of SAO stars having infrared excesses in the *IRAS* Point Source Catalog compiled by Oudmaijer et al. (1992). The color criteria used for determining that a star had an infrared excess were $[12] - [25] > 0.4$ or $[25] - [60] > 0.3$. We selected our sources from this list using the additional criteria that the stars were of spectral types A–K and on the main sequence. Out of the 462 stars in the Oudmaijer et al. (1992) list, approximately 12% met our criteria. Out of those stars, we ultimately observed only six due to the observability of the sources, the elimination of sources that had already been studied extensively in the submillimeter (e.g., Vega and Fomalhaut) as well as any sources showing evidence of emission lines (e.g., Herbig Ae/Be stars), and time

constraints. Although not listed in Oudmaijer et al. (1992) as a Herbig Ae/Be star, HD 37357 has been identified as a Herbig Ae star with spectral type A0 Ve (Thé, de Winter, & Pérez 1994); we have retained it in our source list for comparison purposes. Additionally, β Leo had been observed previously in the submillimeter (Weintraub & Stern 1994) to have a 3 σ upper limit of 21.3 mJy at 1300 μm. We applied the Oudmaijer et al. (1992) color-magnitude criterion to our *SIRTF* SRD sources and found that HD 10700 also possesses an infrared excess.

Table 1 provides a listing of all of the sources we observed at the SMTO, and Table 3 shows the *IRAS* fluxes or upper limits obtained for each source. For our nondetections, we calculated 3 σ upper limits for the flux (Table 2) and 3 σ limits for the mass of dust that could be present in these disks (Table 4). These limits will help constrain the spectral energy distributions of the stars and will be useful comparisons for future observations with *SIRTF*. For the case of HD 131156, our one 3 σ detection at 1300 μm, we give a flux and calculate a minimum dust mass for the system.

3. SUBMILLIMETER RESULTS

Blackbody and graybody fits to the SED of each candidate star are shown in Figures 1 and 2. The solid curve corresponds to a blackbody appropriate for the star's spectral type, scaled to the expected stellar flux for its observed visual magnitude (*open diamond*). For uniformity, we elected to simply scale the stellar blackbodies to the visual magnitudes since Two Micron All Sky Survey magnitudes are not available for many of our stars and some of our sources have an excess at 12 μm, so we cannot scale the stellar photosphere to the *IRAS* data. We used blackbodies instead of sophisticated stellar atmospheric models since all but one of our fluxes are upper limits and the contribution of the stellar photosphere at submillimeter wavelengths is expected to follow a Rayleigh-Jeans slope. For our one source for which we have a detection, HD 131156, we also plot the SMTO and Palomar results in comparison with a Kurucz stellar atmosphere model in Figure 3.

In all of the plots, the *IRAS* flux densities or upper limits (at 12, 25, 60, and 100 μm) are color-corrected in a process

TABLE 3
IRAS FLUXES OR UPPER LIMITS (IN Jy)

Star	12 μm	25 μm	60 μm	100 μm
HD 10700[a]	9.562 ± 0.669	2.157 ± 0.194	0.513 ± 0.056	<1.360
HD 165341...............	7.374 ± 0.295	1.805 ± 0.144	<0.400	<1.348
HD 185144...............	3.313 ± 0.100	0.744 ± 0.060	<0.400	<4.099
HD 4614	7.609 ± 0.380	1.746 ± 0.105	<0.400	<1.841
HD 131156...............	4.086 ± 0.286	0.964 ± 0.077	<0.400	<1.000
HD 32923[a]	1.924 ± 0.115	0.550 ± 0.072	<0.400	<6.908
HD 192425[a]	0.497 ± 0.035	0.235 ± 0.033	<0.400	<1.135
HD 82189[a]	0.612 ± 0.037	0.301 ± 0.238	<0.400	<1.062
HD 39415[a]	0.30 ± 0.03	0.27 ± 0.09	<0.40	<1.23
HD 37357[a]	2.01 ± 0.121	2.79 ± 0.195	2.90 ± 1.537	20.29 ± 2.638
HD 102647[a]	6.970 ± 0.349	2.107 ± 0.232	1.179 ± 0.130	<1.000

NOTE.—Listed above are the sources' *IRAS* fluxes from the *IRAS* Point Source Catalog ver. 2.1 before color correcting. If no error is listed, the flux is an upper limit.

[a] Star has an infrared excess.

that calculates the color-corrected photospheric and dust components separately (Holmes 2002). These photospheric and dust components are plotted in Figures 1 and 2. In many cases, especially at 12 and 25 μm, the dust components are essentially zero. Blackbodies (corresponding to large grains) and graybodies (appropriate for small grains) are then fitted to the color-corrected infrared dust component (or upper limit to the dust component) of each star. A graybody is defined as a modified blackbody in which the emissivity, ϵ, is a function of wavelength: $\epsilon \sim \lambda^{-\beta}$ (where $\beta = 1$, 2). Vega-type disks are expected to have $1 \leq \beta \leq 2$ on the basis of previous observations (Walker & Heinrichsen 2000). Ideally, the best fit would include all of the *IRAS* flux densities, but that is not always possible since most sources possess only upper limits in the 60 and 100 μm wave bands. In some of these cases, there is no discernible 12 μm excess, and a fit must be made using just the 25 μm flux density and one or both of the 60 or 100 μm upper limits.

For each source, the 3 σ upper limits obtained from SMTO are plotted on their respective SEDs. Depending on how well the blackbody or graybodies are fitted to the dust component of the *IRAS* data and depending on where the upper limits from the SMTO data lie on the graybody or blackbody curves, the likelihood of the presence of dust in the system can be assessed. The fits to the dust component give a temperature for the dust component, T_{dust}, which can be used to estimate the mass of dust in the system, M_{dust}. However, if T_{dust} is too low, it could be an indication that the SMTO upper limits are placing limits on infrared cirrus in the background instead of on dust in the system. For instance, the temperature of the warm component of infrared cirrus in the 100 μm wave band is estimated to be approximately 22.5 K (Paley et al. 1991). It is important to recognize the quality of the fit to the dust component of the *IRAS* fluxes in assessing the significance of the SMTO upper limits. We fitted blackbodies and graybodies to the dust components by assuming all of the dust in the system is at one temperature, T_{dust}. A poor fit could be explained by a system that, like the solar system, has two dust components—a warm component analogous to the zodiacal cloud and a colder component similar to the Kuiper belt, which would require three different blackbody curves to explain the SED. It is also possible that some stars do not have a dust component.

TABLE 4
DUST MASS VALUES OR 3 σ LIMITS

STAR	DISTANCE (pc)	STELLAR AGE	T_{dust} ($\beta = 0$) (K)	3 σ LIMITS ON DUST MASS (M_{moon}) 870 μm	1300 μm
HD 10700	3.65	7 Gyr	60	<0.11	
HD 165341..............	5.09		63		<1.2
HD 185144..............	5.77	5.5 Gyr	23	<1.8	<2.0
HD 4614	5.95		25	<1.2	<12
HD 131156..............	6.70		39	<0.54	2.4 ± 0.7
HD 32923	15.9		85	<2.8	<12
HD 192425..............	47.1		79	<23	<69
HD 82189	49.9		100		<68
HD 37357	∼480	≤6 Myr	156	<1300	<12,000
HD 102647..............	11.1	240 Myr	104	<0.59	<3.2

NOTE.—Ages are obtained from Lachaume et al. 1999 except for HD 37357, which is taken from Strom et al. 1989. For comparison, the dust masses of Vega, Fomalhaut, and β Pic were estimated to be 0.7, 1.5, and 7.8 lunar masses, respectively, from 850 μm observations at the James Clerk Maxwell Telescope using SCUBA; see Holland et al. 1998.
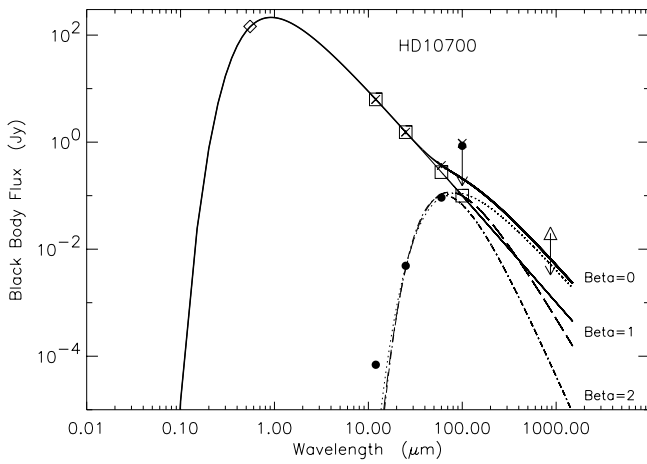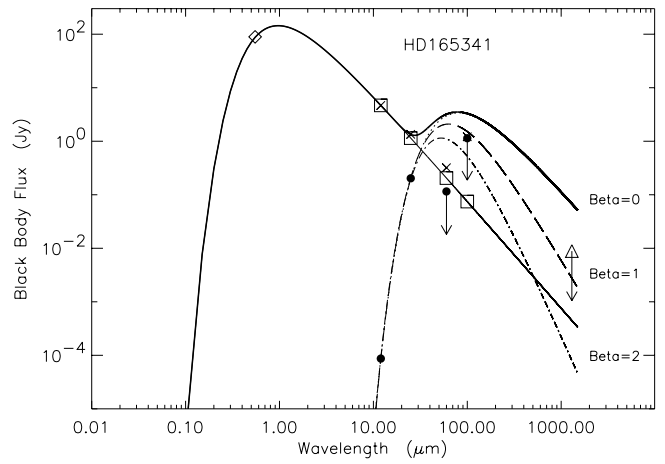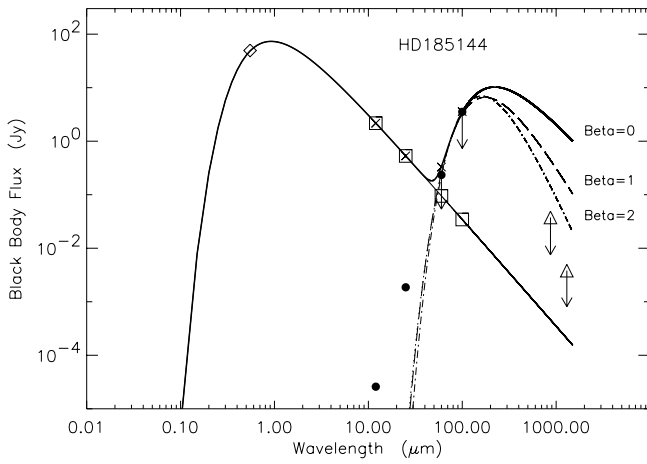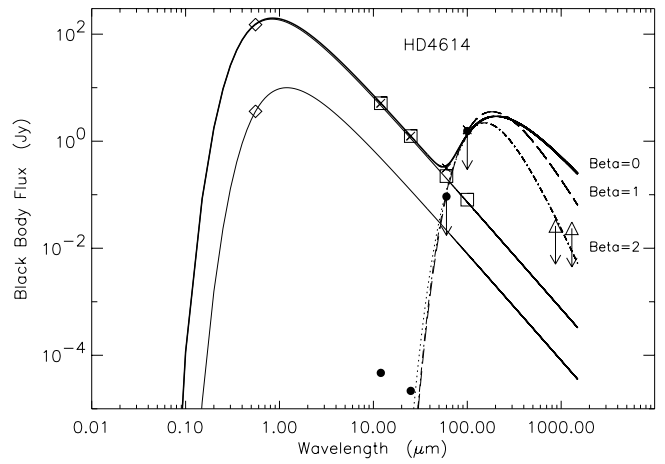
FIG. 1a

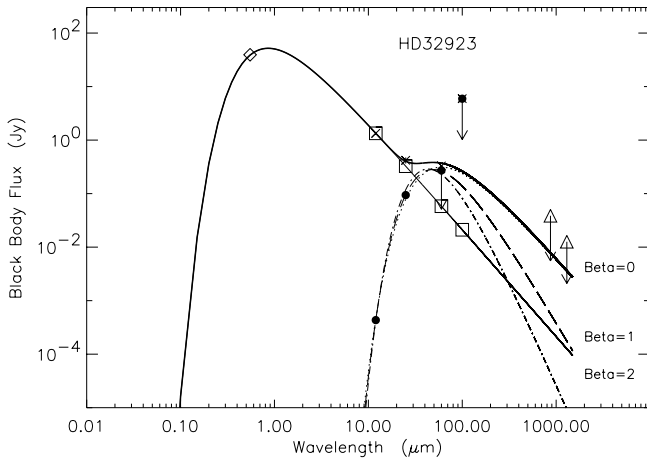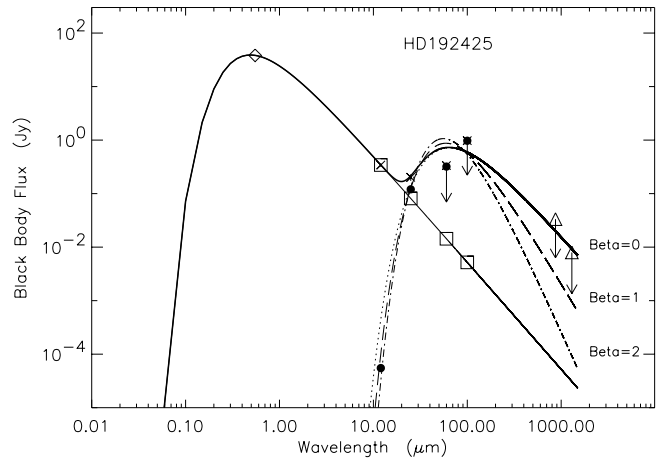FIG. 1b

FIG. 1c

FIG. 1d

FIG. 1e

FIG. 1f

FIG. 1.—Blackbody ($\beta = 0$) and graybody ($\beta = 1$ and 2) fits to the color-corrected dust component of the *IRAS* fluxes for (*a*) HD 10700, (*b*) HD 165341, (*c*) HD 185144, (*d*) HD 4614, (*e*) HD 32923, (*f*) HD 192425, (*g*) HD 82189, (*h*) HD 37357, (*i*) HD 39415, and (*j*) HD 102647 (β Leo). A graybody is defined as a modified blackbody in which the emissivity, ϵ, is a function of wavelength: $\epsilon \sim \lambda^{-\beta}$ (where $\beta = 1, 2$). The open diamonds are fluxes derived from the visual magnitudes given in Table 1. The total color-corrected *IRAS* fluxes or upper limits are represented by crosses. The stellar photospheric component of the *IRAS* fluxes/upper limits are denoted by open squares, the dust component of the *IRAS* fluxes are shown as filled circles, and the dust component of the *IRAS* upper limits are shown as filled circles with arrows. Open triangles denote SMTO fluxes or 3 σ upper limits from observations at 870 and 1300 μm. The blackbody values of the stellar photosphere are plotted as a solid line. In the case of binary stars for which there is information on both components, both photospheric components are plotted. The blackbody and graybody fits to the dust are also plotted: the $\beta = 0$ curve as a dotted line, the $\beta = 1$ curve as a dashed line, and the $\beta = 2$ curve as a dash-dotted line. The thick solid line represents the addition of the stellar photosphere curve(s) and the $\beta = 0$ blackbody fit to the dust component. In the case of β Leo (HD 102647), the asterisk represents the 3 σ upper limit obtained by Weintraub & Stern (1994).
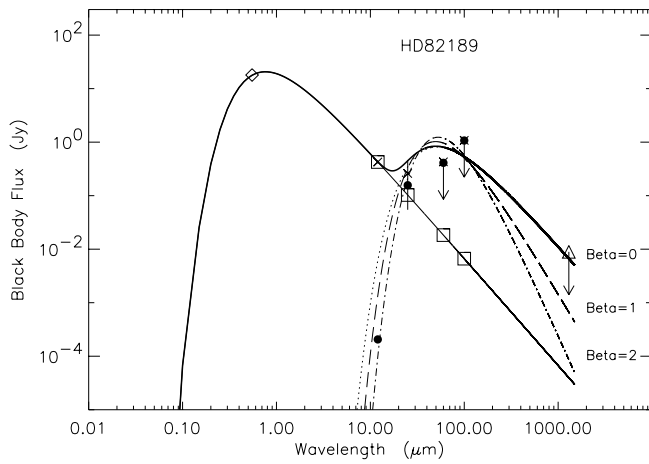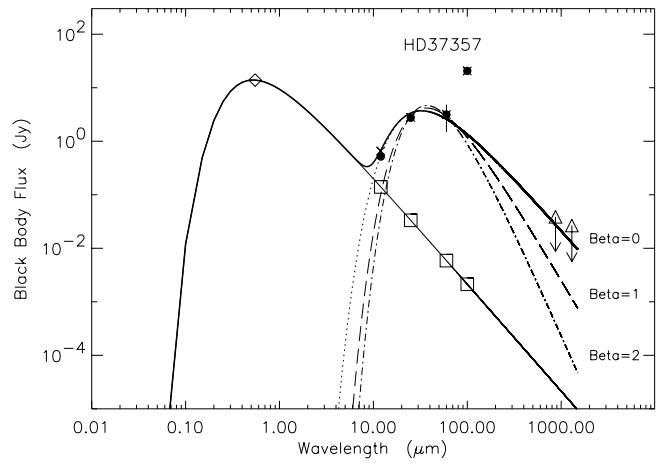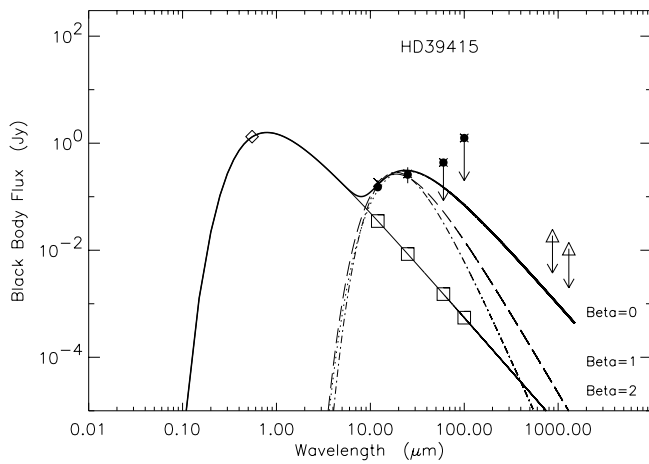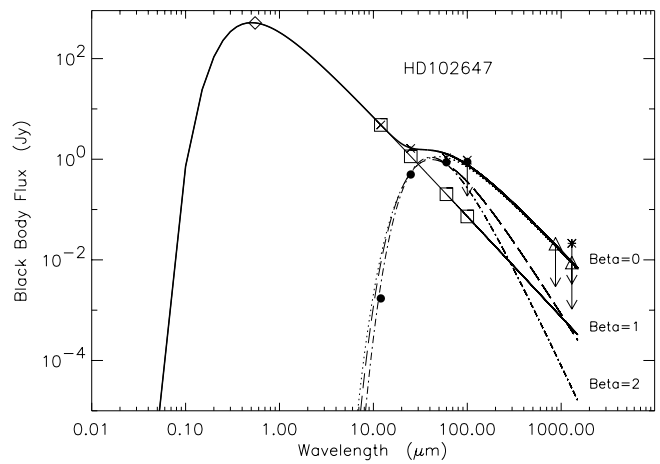
FIG. 1g

FIG. 1h

FIG. 1i

FIG. 1j

3.1. *Sources with Infrared Excesses*

The blackbody and graybody curves for HD 10700 (Fig. 1a), HD 32923 (Fig. 1e), HD 37357 (Fig. 1h), HD 39415 (Fig. 1i), and HD 102647 (Fig. 1j) display a good fit to the color-corrected dust component of the *IRAS* fluxes, clearly indicating the existence of an infrared excess. The *IRAS* 60 and 100 μm dust component fluxes or upper limits are on or clearly above the $\beta = 0$ SED and the 3 σ SMTO upper limits are also clearly above the $\beta = 0$ SED. The implication is that there is a significant probability of dust in the system and that the presence of dust detectable at submillimeter wavelengths cannot be ruled out. These stars would be excellent candidates for more sensitive instruments such as *SIRTF* (in the mid- and far-infrared) and the Submillimeter Array (SMA). The two remaining *IRAS* infrared excess sources, HD 192425 (Fig. 1f) and HD 82189 (Fig. 1g), have no discernible 12 μm excesses and small 25 μm excesses that were used to fit the blackbody curves.

3.1.1. *HD 10700*

For HD 10700 (Fig. 1a), the 60 μm *IRAS* flux is above the Rayleigh-Jeans slope of the blackbody curve, indicating that there may be a small dust component. Both the *IRAS* upper limit at 100 μm and the SMTO upper limit at 870 μm are clearly above the blackbody curve and the curve

combining both the photospheric emission and the dust component.

3.1.2. *HD 32923*

The SED for HD 32923 (Fig. 1e) also makes a convincing case for a dust component. The 25 μm infrared excess of HD 32923 can clearly be seen in Figure 1e. Both the *IRAS* and SMTO upper limits fall on or above the blackbody curve.

3.1.3. *HD 192425 and HD 82189*

HD 192425 (Fig. 1f) and HD 82189 (Fig. 1g) do not have 12 μm excesses and have small 25 μm excesses that were used to fit the blackbody curves. However, in both cases, the 60 μm upper limits were below all of the blackbody fits for dust emission, implying either that there is no emission from dust at longer wavelengths or that these sources have both a warm dust component and a colder dust component. The SMTO 3 σ upper limits were all above the $\beta = 1$ curves and far above the photospheric blackbody curve. HD 192425 has a small 25 μm excess. HD 82189 has a larger excess at 25 μm, but the error bar on the measurement is large—79% of the 25 μm flux. It is possible that these systems possess debris disks, but is also important to keep in mind that a small infrared excess may not be due to a circumstellar disk but instead to a background object in the large *IRAS* beam.
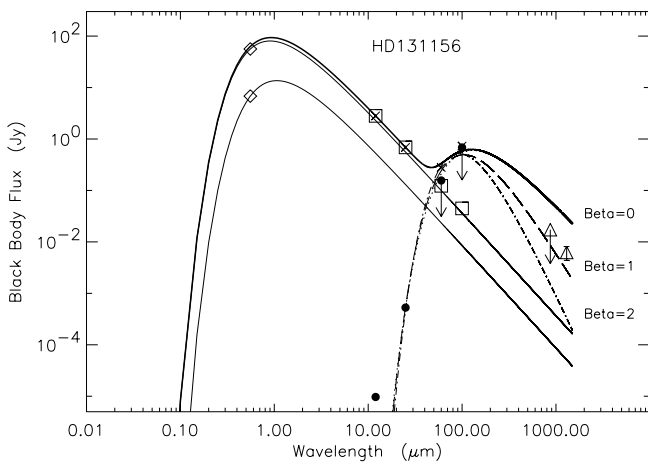
FIG. 2.—Blackbody ($\beta = 0$) and graybody ($\beta = 1$ and 2) fits to the dust component of the color-corrected *IRAS* fluxes and upper limits for HD 131156. The symbols are the same as in Fig. 1. Our one 3 σ detection (S/N = 3.33), HD 131156, has a mean flux of 6.25 ± 1.88 mJy and a corresponding dust mass of 2.4 ± 0.7 lunar masses. For comparison, the total mass in the observable Kuiper belt is of order 0.1 Earth masses, corresponding to approximately 8.2 lunar masses (Jewitt, Luu, & Chen 1996; Jewitt et al. 1998; Luu & Jewitt 1998).

Overall, we consider the blackbody and graybody curves to be a fair fit to the *IRAS* data.

3.1.4. *HD 37357*

HD 37357 (Fig. 1*h*) is different from the other main-sequence stars on our list because it has been identified as a Herbig Ae star with spectral type A0 Ve (Thé et al. 1994). Strom et al. (1989) classified HD 37357 as a class II source, meaning the slope of the SED is intermediate between a blackbody and a flat spectrum. The star is associated with the Lynds 1641 dark cloud, which is the nearest giant molecular cloud at a distance of 480 pc. The A_V for HD 37357 was found to be 2.8 (Strom et al. 1989), yielding a visual magnitude corrected for extinction, m_V, of 6.05. HD 37357 was detected at all four *IRAS* wave bands, and the detections indicate that the star possesses a large circumstellar dust disk. The *IRAS* flux qualities for the 12 and 25 μm fluxes were 3, or " good," and the 60 and 100 μm flux qualities were 2, or " moderate." In general, we tried to fit to the longer wavelengths preferentially, but since Strom et al. (1989) noted that the 100 μm flux was hard to measure, we decided to exclude the 100 μm flux from our fit to the HD 37357 data. The SMTO 3 σ upper limits fall on the blackbody curve.

3.1.5. *HD 39415*

HD 39415 (Fig. 1*i*) clearly has an infrared excess at both 12 and 25 μm, and the upper limits for both *IRAS* and SMTO are above the blackbody curve. The on-source integration time for both SMTO wave bands was approximately an hour, but we were still unable to either detect any submillimeter emission or get an upper limit down to the stellar photosphere. With *SIRTF*'s anticipated sensitivity, this star would make an excellent candidate for MIPS observations at 70 and 160 μm.

3.1.6. *HD 102647* (β *Leo*)

β Leo (Fig. 1*j*) has an infrared excess at 25 and 60 μm, and the 100 μm *IRAS* upper limit and the SMTO upper

limits all lie on the $\beta = 0$ curve. We compare our 3 σ upper limit at 1300 μm for β Leo with the 3 σ upper limit obtained by Weintraub & Stern (1994), which is represented in Figure 1*j* as an asterisk. We find that our upper limit is more than a factor of 2 lower than that obtained by Weintraub & Stern (1994).

3.2. *Other Sources*

The remaining four sources (HD 165341, HD 185144, HD 4614, and HD 131156) are not listed in Oudmaijer et al. (1992) as *IRAS* excess sources, although from our color-correcting process, it is possible that HD 165341 may have a marginal 25 μm excess.

3.2.1. *HD 131156*

The SED of HD 131156 (Fig. 2) is the most interesting because of our 3 σ detection at 1300 μm. This binary system is composed of stars with spectral types of G8 V and K4 V (Fernandes et al. 1998) and masses of 0.85 and 0.72 $M_\odot$. They are separated by approximately 7″ and have a period of 151 yr (Gray et al. 1996 and references therein). Their small angular separation is much less than the SMTO beam size for both wavelengths. The 60 μm *IRAS* upper limit, although above the stellar photospheres, falls slightly below the $\beta = 0$ blackbody curve. However, this could simply mean that the dust component is best fitted not with a single temperature but with a warm inner disk and a cold outer disk, or with only a cold outer disk. Both the 3 σ upper limit at 870 μm and the 3 σ detection at 1300 μm lie above the $\beta = 1$ blackbody curve and well above the stellar photosphere. Infrared observations of this source taken at Palomar with MIRLIN are discussed in § 5.

3.2.2. *HD 165341*

Overall, the fit to the *IRAS* data and upper limits for HD 165341 (Fig. 1*b*) is poor, but the fact that our color-correction process has yielded a small 25 μm excess supports the existence of a dust component. However, the total *IRAS* 60 μm upper limit is only marginally above the blackbody curve for the stellar photosphere, which may mean that there is no cold dust component or the amount of cold dust is very small. The SMTO 3 σ upper limit for HD 165341 is low, above the $\beta = 1$ curve, but not much greater than the stellar photosphere curve, making this source a poor candidate for possessing a large cold dust component.

3.2.3. *HD 185144*

The fits to the dust component of the *IRAS* 60 and 100 μm upper limits for HD 185144 (Fig. 1*c*) is reasonably good, although it could merely be due to a spuriously high 100 μm upper limit since there is no excess emission at 12 or 25 μm. However, the 3 σ SMTO upper limits are both below the $\beta = 2$ curve, which makes a cold dust component very unlikely if it has the same temperature as dust at 60 and 100 μm. We also note that $T_{\rm dust}$ is 23 K, which is lower than one would expect for a typical dust component.

3.2.4. *HD 4614*

In the case of the spectroscopic binary HD 4614 (Fig. 1*d*), there is no 12 or 25 μm excess, and the total *IRAS* 60 μm upper limit is only marginally above the blackbody curve for the stellar photosphere. The 12 and 25 μm fluxes, as well as the 60 μm upper limit, are nearly coincident with the

blackbody curve for the stellar photosphere, and the SMTO upper limits are at or below the $\beta = 2$ curves, which makes a cold dust component unlikely. Finally, we also note that T_{dust} is 25 K, which is low for a typical dust component.

4. DUST MASS

The envelopes or disks surrounding many young stars contain gas and dust, both of which contribute to the measured mass. However, in the case of the more evolved planetary debris disks, most of the gas has been cleared away, as evidenced by the null results from searches for gas around Vega-type stars. The gas-to-dust ratio in these debris disks is reported to be at least 10–1000 times lower than in the interstellar medium (Dent et al. 1995; Freudling et al. 1995). For this paper, we adopt a gas-to-dust ratio that is 100 times less than that found in the interstellar medium (ISM), which translates into adopting a mass absorption coefficient, K_{abs}, for our systems, which is 100 times greater than for a system with an assumed gas-to-dust ratio appropriate for the ISM. We calculated a dust mass for HD 131156 and 3 σ limits on dust mass around the remaining stars using the following equation from Zuckerman & Becklin (1993),

$$M_{dust} = \frac{F_\nu d^2}{B(\nu, T_{dust})K_{abs}} , \quad (1)$$

where M_{dust} is in grams, F_ν is the flux or the 3 σ upper limit to the flux in janskys, d is the distance to the star in meters, and K_{abs} is the mass absorption coefficient in units of m^2 g^{-1}. The blackbody intensity, $B(\nu, T_{dust})$, is measured in janskys, and T_{dust} is the temperature of the dust grains in kelvins; T_{dust} was derived from a blackbody ($\beta = 0$) fit to the color-corrected dust component of the *IRAS* fluxes (see Table 4).

In the low-temperature submillimeter regime, $B(\nu, T_{dust})$ can be approximated by $2kT_{dust}/\lambda^2$ in the Rayleigh-Jeans limit (Zuckerman & Becklin 1993; Hildebrand 1983), which is advantageous since in this approximation M_{dust} depends only inversely on the uncertain dust temperature. However, the Rayleigh-Jeans limit is inappropriate for dust temperatures less than or equal to 50 K (Weintraub & Stern 1994), and from some of our fits we obtained a T_{dust} lower than 50 K. We calculated 3 σ limits for the dust mass around the candidate stars using both the full blackbody expression and the Rayleigh-Jeans limit and found a 6%–10% difference in the results. As a result, we decided to use the full expression for blackbody intensity for our dust mass calculations.

The 3 σ limits for the dust masses in the observed systems are given in Table 4 in units of lunar masses (M_{moon}). The mass absorption coefficient, K_{abs}, can vary by up to a factor of 4 in the wavelength regime we are considering (Pollack et al. 1994), and it must be noted that because of the uncertainty in K_{abs} and the uncertainty in the power-law size distribution of the dust, our limits for dust mass are order-of-magnitude estimates. The mass absorption coefficient is not well constrained since it depends on the undetermined sizes of the dust particles presumed to be orbiting around the star. We use a K_{abs} for 1300 μm of 0.29 cm^2 g^{-1} (Pollack et al. 1994; Zuckerman & Becklin 1993). This value for the mass absorption coefficient is derived assuming that the flux comes from particles with a diameter approximately equal to 600 μm, so our estimates represent a minimum dust mass

for the large grain case. For consistency with the results of Holland et al. (1998), we choose a K_{abs} for 870 μm of 1.7 cm^2 g^{-1}, which is appropriate for large particles of diameter $\sim$600 μm (Holland et al. 1998; Zuckerman & Becklin 1993), again giving us a minimum dust mass.

Our 3 σ limits on dust mass at 870 μm are easily compared with the values obtained by Holland et al. (1998). From our list of candidates, HD 10700, HD 185144, HD 4614, HD 131156, HD 32923, and β Leo show limits on dust masses at 870 μm on the order of the masses of Vega and Fomalhaut ($0.11 \leq M_{dust} \leq 2.8$ lunar masses). The mass limits at 1300 μm are not as tight, due to the fact that the four-color bolometer is not as sensitive as the 19 channel bolometer array. However, they still show that for five of our sources, the limits and detection are on the order of previously observed debris disks ($1.2 \leq M_{dust} \leq 12$ lunar masses). The masses of HD 192425 and HD 82189 are poorly constrained, most likely because of their large distances, although as a Herbig Ae star, HD 37357 is expected to have a dust mass that is much larger than a typical planetary debris disk.

4.1. *HD 131156*

Our one 3 σ detection, HD 131156, has a flux of 6.25 ± 1.88 mJy at 1300 μm and a corresponding minimum dust mass of 2.4 ± 0.7 lunar masses. Holland et al. (1998) found dust masses for Vega, Fomalhaut, and β Pic of 0.7, 1.5, and 7.8 lunar masses, respectively. As another comparison, the total mass in the observable Kuiper belt is approximately 8.2 lunar masses (Jewitt, Luu, & Chen 1996; Jewitt et al. 1998; Luu & Jewitt 1998). The dust mass for HD 131156 fits in well with these estimates.

4.2. *HD 37357*

Converting the upper limits on dust mass for HD 37357 in Table 4 from lunar masses to solar masses yields 4.9×10^{-5} $M_\odot$ at 870 μm and 4.3×10^{-4} $M_\odot$ at 1300 μm. Since HD 37357 is a Herbig Ae/Be star, we assume an ISM gas-to-dust ratio and calculate a 3 σ limit on gas and dust of 0.0049 $M_\odot$ for 870 μm and 0.043 $M_\odot$ for 1300 μm, which is similar to observations of other Herbig Ae/Be circumstellar disks (Natta, Grinin, & Mannings 2000).

5. INFRARED OBSERVATIONS OF HD 131156

We performed follow-up mid-infrared observations on HD 131156 using the Jet Propulsion Laboratory (JPL) Mid-InfraRed Large Imager (MIRLIN) (Ressler et al. 1994), at the Palomar 200 inch (5 m) diameter telescope on 2002 April 29 (UT). MIRLIN is an infrared camera that uses a 128×128 pixel Boeing HF-16 Si:As impurity band conductor detector array. The measured plate scale is approximately 0.″15 pixel^{-1} at the Palomar 200 inch telescope (Ressler et al. 1994). The chopper throw was 7″, and the telescope was nodded ±5″ east and north to perform background subtraction. Our standards for 2002 April 28–30 were α Boo, Vega (α Lyr), μ UMa, and β Gem. On the night of April 29, HD 131156 was observed with the N, N0, N1, N2, N3, N4, and N5 MIRLIN filters that correspond to wavelengths of 10.8, 7.9, 8.8, 9.7, 10.3, 11.7, and 12.5 μm.

The MIRLIN data were processed using two independent methods: the in-house IDL Match And Combine routine (MAC), developed specifically for use with MIRLIN data by K. A. Marsh and updated by various collaborators, and

TABLE 5
MIRLIN DATA FOR HD 131156

Filter	λ (μm)	HD 131156 A Flux (Jy)	HD 131156 B Flux (Jy)
N0.................	7.9	6.83 ± 0.45	1.80 ± 0.12
N1.................	8.8	5.31 ± 0.35	1.42 ± 0.09
N2.................	9.7	4.16 ± 0.27	0.965 ± 0.071
N3.................	10.3	3.77 ± 0.24	1.008 ± 0.067
N	10.8	3.40 ± 0.22	0.915 ± 0.059
N4.................	11.7	2.69 ± 0.18	0.800 ± 0.055
N5.................	12.5	2.16 ± 0.15	0.658 ± 0.060

IRAF DAOPHOT routines. Circular aperture photometry was performed on both the targets, and the standards were taken throughout the night using an aperture of radius of 13 pixels. Extinction measurements were obtained from observations of μ UMa on 2002 April 29. The final MIRLIN flux values are given in Table 5. We assume an absolute calibration uncertainty of 6% for the MIRLIN photometry in addition to the statistical errors due to photon statistics and scatter in air-mass fits.

In Figure 3, *U*-, *B*-, *V*-, *I*-, *J*-, *K*-, and *L*-band photometry from the literature are shown as squares. For both stellar components *B* and *V* are *Hipparcos* magnitudes. The *U*- and *I*-band magnitudes for HD 131156 A are taken from Johnson et al. (1966), and the *J*-, *K*-, and *L*-band magnitudes are obtained from Johnson, McArthur, & Mitchell (1968). The *U*-band magnitude for HD 131156 B is from Lutz (1971). The solid lines are Kurucz model atmospheres fitted to the *U*-, *B*-, *V*-, *I*-, *J*-, *K*-, and *L*-band photometry. Fluxes derived from *Hipparcos* data are assumed to have 2% errors, while the *U*-, *I*-, *J*-, *K*-, and *L*-band fluxes derived
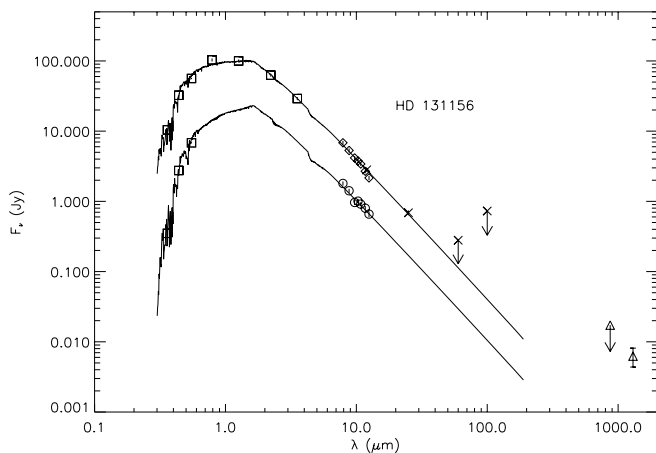
from the literature are assumed to have 5% errors. The best-fit Kurucz model for HD 131156 A is a K0 V spectral type ($T_{\rm eff} = 5250$ K) with a normalization factor of $(14.323 \pm 0.280) \times 10^6$ and a reduced χ^2 of 2.66. The best-fit Kurucz model for HD 131156 B is a K4 V spectral type ($T_{\rm eff} = 4500$ K) with a normalization factor of $(4.308 \pm 0.069) \times 10^6$ and a reduced χ^2 of 2.10. We assumed a metallicity of 0.0 and $\log g = 4.5$ for both stars. The actual spectral types given in Table 1 for HD 131156 A and B are G8 V and K4 V.

The MIRLIN photometry resolves both components of HD 131156. The mid-infrared data are photospheric, implying that the system does not have a hot inner dust component, analogous to the zodiacal cloud. This agrees well with the fact that HD 131156 does not have a 12 μm *IRAS* excess. The system must therefore have an inner hole with a surrounding cold dust component. The SMTO 3 σ detection and upper limit are well above the Kurucz model atmospheres, confirming our earlier results obtained by fitting a blackbody to the data in § 3.

6. CONCLUSIONS AND FUTURE WORK

The blackbody and graybody curves for six of our sources (HD 10700, HD 32923, HD 39415, HD 37357, β Leo, and HD 131156) indicate that the sources are good candidates for having submillimeter excesses. Our one 3 σ detection, HD 131156, has a flux of 6.25 ± 1.88 mJy at 1300 μm and a corresponding dust mass of 2.4 ± 0.7 lunar masses. The dust mass for HD 131156 fits in well with the Holland et al. (1998) results and with the estimated mass of the Kuiper belt $[M_{\rm dust}({\rm Vega}) < M_{\rm dust}$ (Fomalhaut) $< M_{\rm dust}({\rm HD~131156}) < M_{\rm dust}(\beta~{\rm Pic}) < M_{\rm KB}]$. Both the MIRLIN and the *IRAS* 12 and 25 μm data rule out a hot, inner-body component to the HD 131156 system, implying that the system has a sizeable inner hole surrounded by a cold dust component. Both HD 192425 and HD 82189 are fair candidates for having a cold disk component, while we rate HD 165341 between fair and poor. Due to a low $T_{\rm dust}$ and upper limits below or on the $\beta = 2$ curve, HD 185144 and HD 4614 are thought to be poor debris disk candidates.

Including our 3 σ detection, we have no evidence for massive disks surrounding seven of these sources. If disks exist, they may be similar to the tenuous disks surrounding Vega and Fomalhaut, of the order of a lunar mass of material. The mass limits on three of the sources are poorly constrained because of their large (>45 pc) distances, although in the case of the Herbig Ae star, HD 37357, a large dust disk would not be unexpected (Natta et al. 2000).

Our SMTO upper limits constrain the SEDs of the stars and will serve as a comparison with future observations with *SIRTF*, which will have unprecedented sensitivity in the search for emission from planetary debris disks in the infrared. Several already approved programs will observe a statistically significant sample of stars in order to assess the prevalence of debris disks as a function of stellar age, spectral type, binarity, metallicity, and the presence or absence of known planets in the system (Beichman et al. 2003). The programs will do photometry with the Multiband Imaging Photometer (MIPS) for *SIRTF* in the 24, 70, and 160 μm wave bands. Upper limits at wavelengths longward of 160 μm will supplement and constrain the *SIRTF* observations, putting an important limit on the radial extent of the disk and the disk mass.

FIG. 3.—MIRLIN fluxes of HD 131156. *U*-, *B*-, *V*-, *I*-, *J*-, *K*-, and *L*-band photometry from the literature are shown as squares. Color-corrected *IRAS* fluxes and upper limits are shown as crosses. The solid lines are Kurucz model atmospheres fitted to the *U*-, *B*-, *V*-, *I*-, *J*-, *K*-, and *L*-band photometry. *B* and *V* fluxes derived from *Hipparcos* data are assumed to have a 2% error, while *U*-, *I*-, *J*-, *K*-, and *L*-band fluxes derived from the literature are assumed to have a 5% error. HD 131156 was observed with the N, N0, N1, N2, N3, N4, and N5 MIRLIN filters that correspond to wavelengths of 10.8, 7.9, 8.8, 9.7, 10.3, 11.7, and 12.5 μm. MIRLIN data for HD 131156 A are open diamonds, and MIRLIN data for HD 131156 B are circles. The final MIRLIN flux values are given in Table 5. We assume an absolute calibration uncertainty of 6% for the MIRLIN photometry in addition to the statistical errors due to photon statistics and scatter in air mass fits. SMTO data are triangles.

REFERENCES

Aumann, H., & Good, J. 1990, ApJ, 350, 408
Backman, D. E., & Paresce, F. 1993, in Protostars and Planets III, ed. E. H. Levy & J. I. Lunine (Tucson: Univ. Arizona Press), 1253
Beichman, C., Gautier, T. N., Holmes, E. K., Rieke, G., Stansberry, J., Stapelfeldt, K., & Werner, M. 2003, in ASP Conf. Ser., Debris Disks and the Formation of Planets: A Symposium in Memory of Fred Gillet, ed. L. Caroff & D. Backman (San Francisco: ASP), in press
Dent, W. R. F., Greaves, J. S., Mannings, V., Coulson, I. M., & Walther, D. M. 1995, MNRAS, 277, L25
Dermott, S. F., Grogan, K., Holmes, E., & Kortenkamp, S. 1999a, in Formulation and Evolution of Solids in Space, ed. J. M. Greenberg & A. Li (Dordrecht: Kluwer), 565
Dermott, S. F., Grogan, K., Holmes, E. K., & Wyatt, M. C. 1999b, in Proc. Int. Conf. Honouring Heinrich Eichhorn: Modern Astrometry and Astrodynamics, ed. R. Dvorak, H. F. Haupt, & K. Wodnar (Vienna: Austrian Acad. Sci.), 189
Elachi, C., et al. 1996, in A Road Map for the Exploration of Neighboring Planetary Systems (ExNPS), ed. C. Beichman (Tech. Rep.; Pasadena: JPL)
European Space Agency (ESA). 1997, The *Hipparcos* and Tycho Catalogues (ESA SP-1200)
Fernandes, J., Lebreton, Y., Baglin, A., & Morel, P. 1998, A&A, 338, 455
Freudling, W., Lagrange, A. M., Vidal-Madjar, A., Ferlet, R., & Forbeille, F. 1995, A&A, 301, 231
Gillett, F. 1986, in Light on Dark Matter, ed. F. P. Israel (Dordrecht: Reidel), 61
Gray, D. F., Baliunas, S. L., Lockwood, G. W., & Skiff, B. A. 1996, ApJ, 465, 945
Greaves, J. S., et al. 1998, ApJ, 506, L133
Hildebrand, R. H. 1983, QJRAS, 24, 267
Holland, W. S., et al. 1998, Nature, 392, 788
Holmes, E. K. 2002, Ph.D. thesis, Univ. Florida
Holmes, E. K., Dermott, S. F., Grogan, K., & Wyatt, M. C. 1999, in ASP Conf. Ser. 177, Astrophysics with Infrared Surveys: A Prelude to *SIRTF*, ed. M. D. Bicay, C. A. Beichman, R. M. Cutri, & B. F. Madore (San Francisco: ASP), 381

Jewitt, D., Luu, J., & Chen, J. 1996, AJ, 112, 1225
Jewitt, D., Luu, J., & Trujillo, C. 1998, AJ, 115, 2125
Johnson, H. L., Iriarte, B., Mitchell, R. I., & Wisniewski, W. Z. 1966, Comm. Lunar Planet. Lab., 4, 99
Johnson, H. L., McArthur, J. W., & Mitchell, R. I. 1968, ApJ, 152, 465
Koerner, D. W., Ressler, M. E., Werner, M. W., & Backman, D. E. 1998, ApJ, 503, L83
Lachaume, R., Dominik, C., Lanz, T., & Habing, H. J. 1999, A&A, 348, 897
Landgraf, M., Liou, J.-C., Zook, H. A., & Grün, E. 2002, AJ, 123, 2857
Liou, J.-C., & Zook, H. 1999, AJ, 118, 580
Lutz, T. E. 1971, PASP, 83, 488
Luu, J. X., & Jewitt, D. C. 1998, ApJ, 502, L91
Natta, A., Grinin, V. P., & Mannings, V. 2000, in Protostars and Planets IV, ed. V. Mannings, A. P. Boss, & S. S. Russell (Tuscon: Univ. Arizona Press), 559
Oudmaijer, R. D., van der Veen, W. E. C. J., Waters, L. B. F. M., Trams, N. R., Waelkens, C., & Engelsman, E. 1992, A&AS, 96, 625
Paley, E. S., Low, F. J., McGraw, J. T., Cutri, R. M., & Rix, H. 1991, ApJ, 376, 335
Pollack, J. B., Holenbach, D., Beckwith, S., Simonelli, D. P., Roush, T., & Fong, W. 1994, ApJ, 421, 615
Ressler, M. E., Werner, M. W., Van Cleve, J., & Chou, H. A. 1994, Exp. Astron., 3, 277
Sandell, G. 1994, MNRAS, 271, 75
Simmons, L., & Werner, M. 1997, The *Space Infrared Telescope Facility* Science Requirements Document 674-SN-100, Ver. 1.0 (Pasadena: NASA/JPL)
Strom, K. M., Newton, G., Strom, S. E., & Seaman, R. L. 1989, ApJS, 71, 183
Telesco, C. M., et al. 2000, ApJ, 530, 329
Thé, P. S., de Winter, D., & Pérez, M. R. 1994, A&AS, 104, 315
Walker, H. J., & Heinrichsen, I. 2000, Icarus, 143, 147
Weintraub, D. A., & Stern, S. A. 1994, AJ, 108, 701
Zuckerman, B., & Becklin, E. E. 1993, ApJ, 414, 793